Atomic Scale Account of the Surface Effect on Ionic Transport in Silver Hollandite

Xiaobing Hu[a], Jianping Huang[b], Lijun Wu[a], Merzuk Kaltak[c], Maria Victoria Fernandez-Serra[c,d], Qingping Meng[a], Lei Wang[b], Amy C. Marschilok[b,e,f], Esther S. Takeuchi[b,e,f], Kenneth J. Takeuchi[b,e], Mark S. Hybertsen[g] and Yimei Zhu[a]*

[a]*Condensed Matter Physics and Materials Science Department, Brookhaven National Laboratory, Upton, New York 11973, USA*

[b]*Department of Chemistry, Stony Brook University, Stony Brook, New York 11794, USA*

[c]*Department of Physics and Astronomy, Stony Brook University, Stony Brook, New York 11794, USA*

[d]*Institute for Advanced Computational Science, Stony Brook University, Stony Brook, New York 11794, USA*

[e]*Department of Materials Science and Chemical Engineering, Stony Brook University, Stony Brook, New York 11794, USA*

[f]*Energy Sciences Directorate, Brookhaven National Laboratory, Upton, New York 11973, USA*

[g]*Center for Functional Nanomaterials, Brookhaven National Laboratory, Upton, New York 11973, USA*

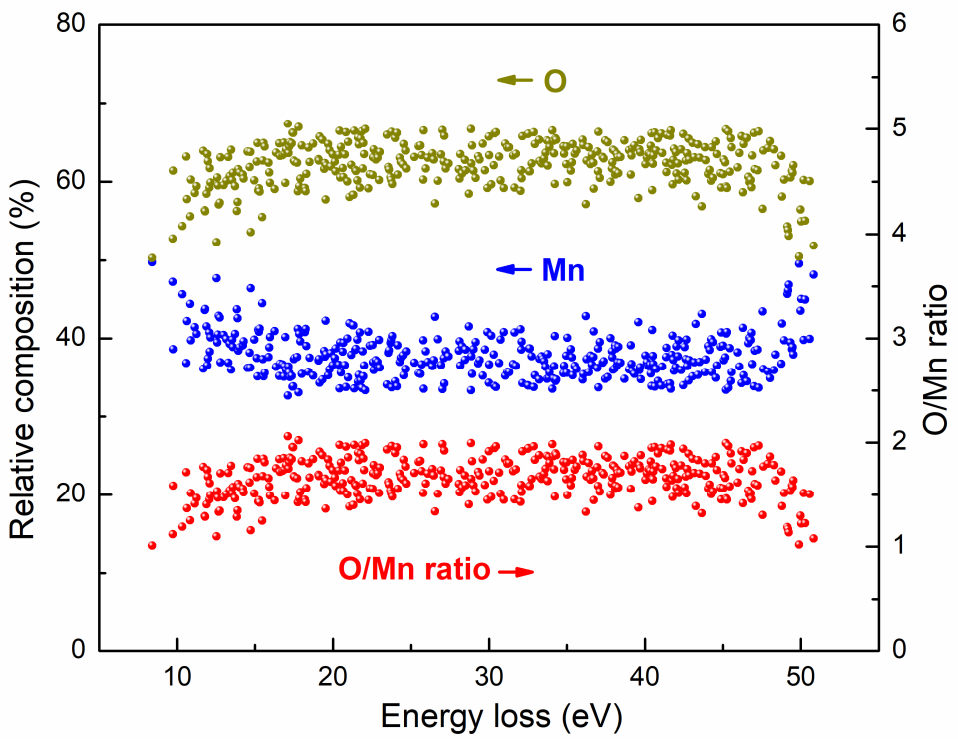

Figure S1. Quantitative analyses of the O, Mn and O/Mn ratio along the nanorod shown in Figure 3a.

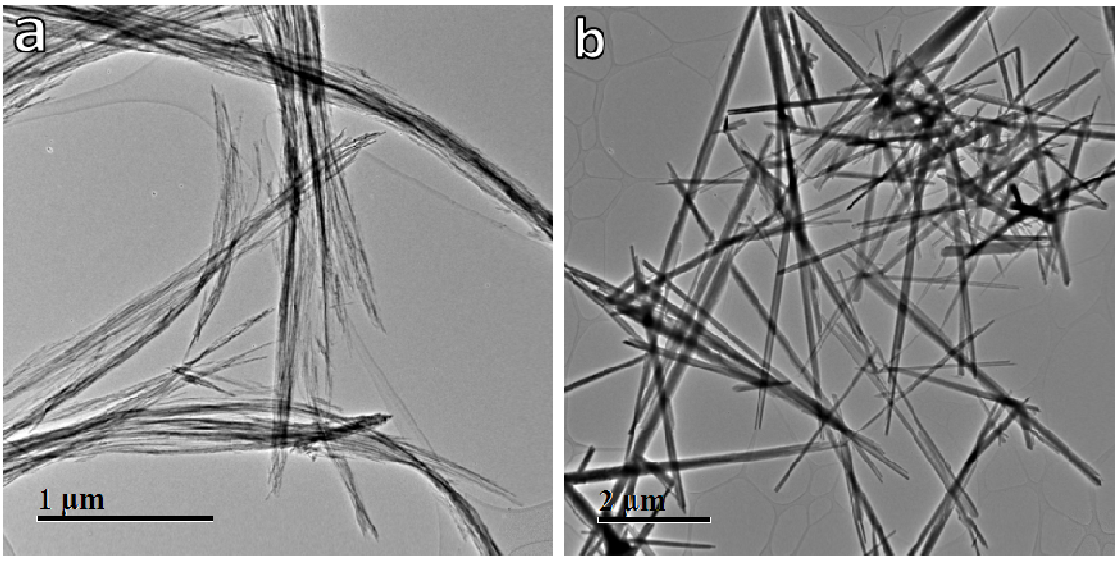

Figure S2. TEM image showing the general morphological features of (a) AgHol-S and (b) AgHol-L samples. The diameter of individual rods for AgHol-S sample is less than 10 nm. However, the diameter for AgHol-L sample ranges from 10 nm to 200 nm.

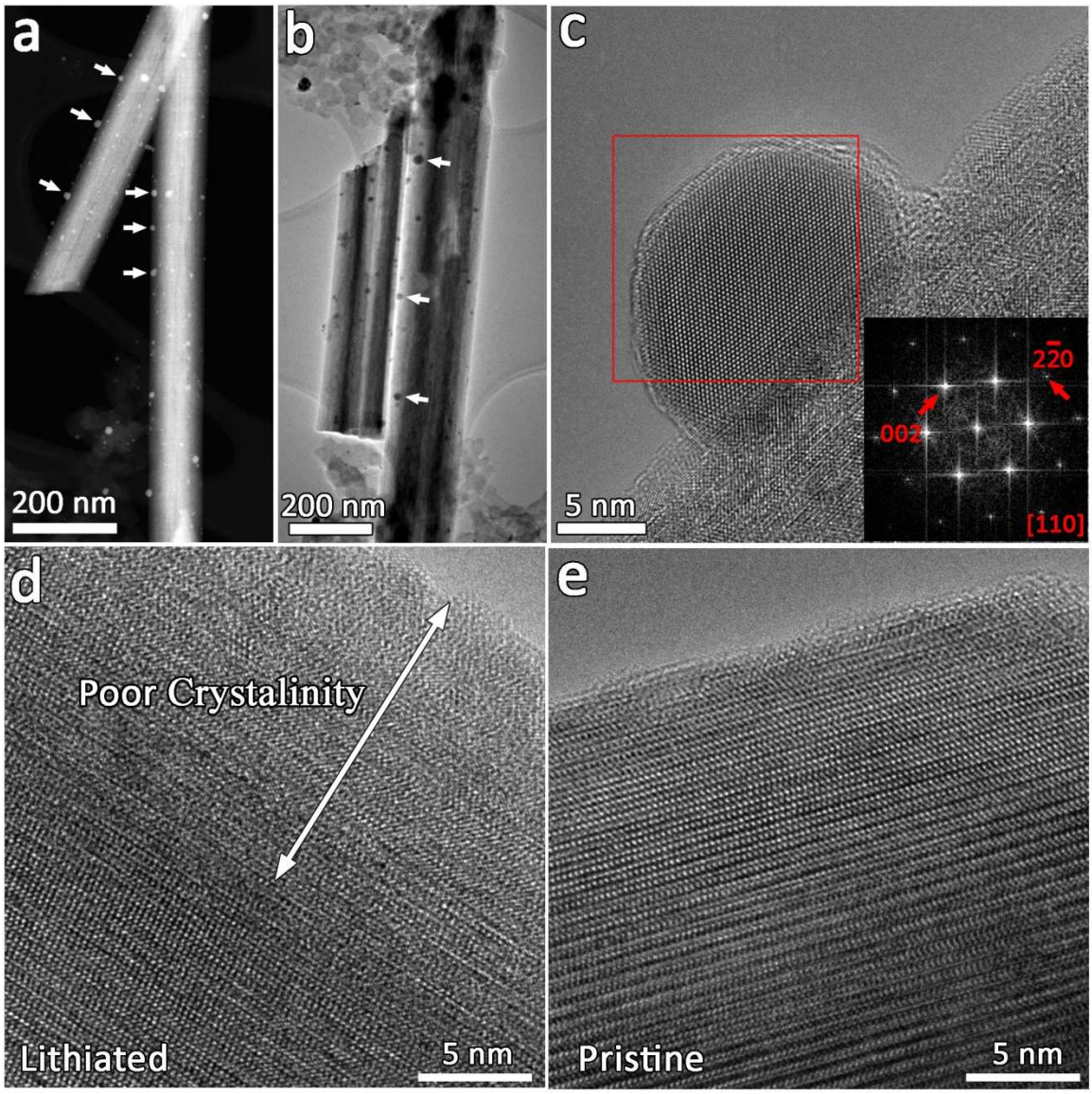

Figure S3. Structural features of lithiated hollandite. Low magnification (a) HAADF and (b) BF images show that the Ag precipitates prefer to form on surface of the rods. On average, the AgHol-L sample is lithiated by 6 Li^+ per unit formula. (c) HRTEM image of the nano-sized Ag

precipitate with its corresponding diffractogram from the region marked by the red square. (d,e) Comparison of HRTEM images between the lithiated and pristine samples show the disorder and poor crystallinity of the surface regions in contrast to interior region of the lithiated rod (d) and the surface region of the pristine rod (e).

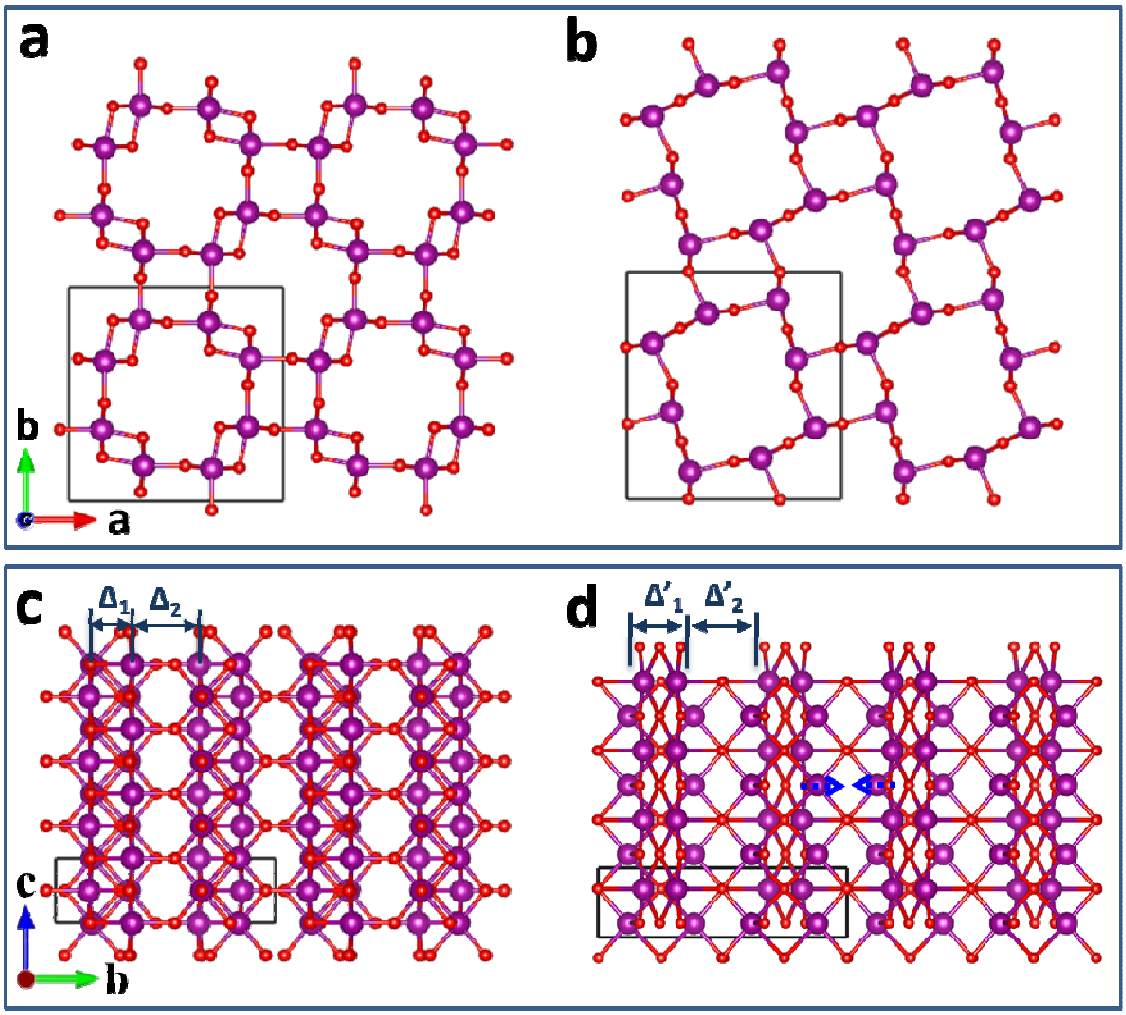

Figure S4. Structural projection of the ideal α-MnO_2 along (a) [001], (c) [100] direction and of the constrained Mn_8O_{12} along (b) [001], (d) [100] direction. The hypothetical reduced structure, Mn_8O_{12}, is found to be metastable with the *a*-axis and *c*-axis lattice parameters fixed to match that of *a*-MnO_2 and *b*-axis lattice parameter allowed to relax. The arrows in (d) indicated relative

shift of Mn columns because of O vacancy in contrast to that of the ideal structure. The averaged interlayer distance Δ_1 and Δ_2 in the relaxed α-MnO_2 structure are indicated and measured as 1.75 Å and 3.02 Å respectively. The averaged interlayer distance Δ'_1 and Δ'_2 in the relaxed Mn_3O_4 model structure are measured as 2.45 Å and 2.89 Å respectively.

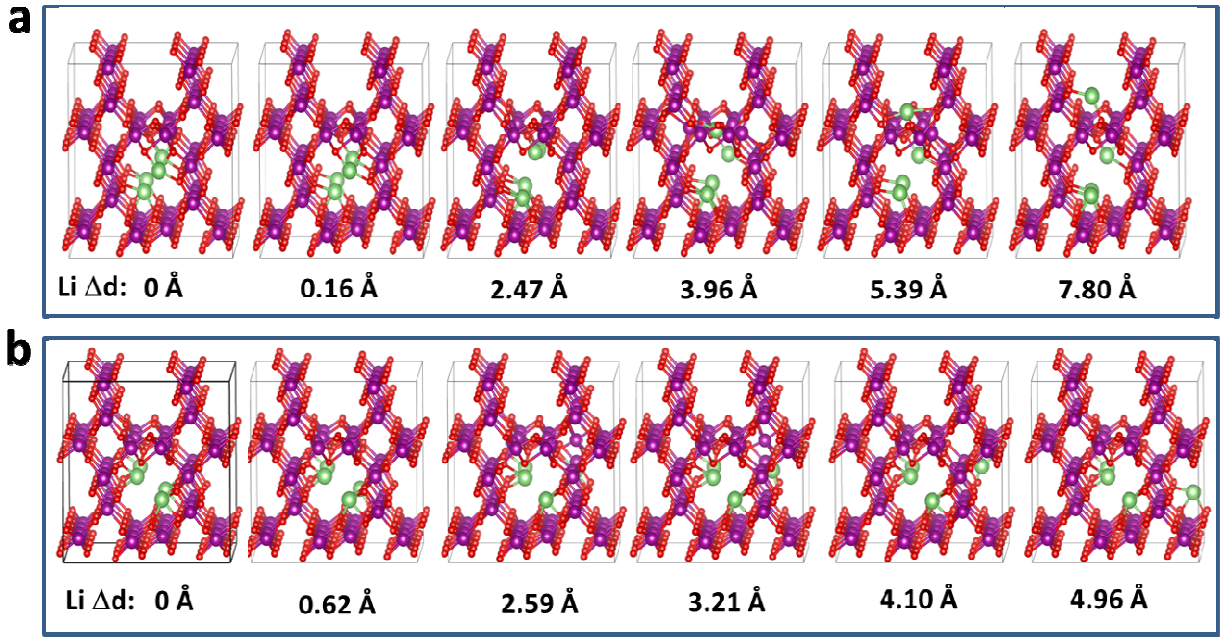

Figure S5. The initial and final structures, together with selected intermediate structures, corresponding to the energy barrier calculations probing the diffusion process of Li through (a) wall with a double O vacancy and (b) intact wall, all in the $\sqrt{2}\times\sqrt{2}\times4$ supercell with composition $Li_4Mn_{64}O_{126}$. Distance along the reaction pathway, measured by the displacement of the active Li ion, is noted for each structure.